JOURNAL OF PROPULSION AND POWER
Vol. 23, No. 1, January–February 2007

Modeling of Propellants Containing Ultrafine Aluminum

T. L. Jackson, J. Buckmaster,* and X. Wang
University of Illinois, Urbana, Illinois 61801

DOI: 10.2514/1.17493

In the study of heterogeneous propellants that contain large amounts of fine aluminum and ammonium perchlorate, it is appropriate to distinguish between the matrix (a homogenized blend of fine particles and binder) and larger particles that are embedded in this matrix. Then the burning properties of a pure matrix are required. We construct a one-dimensional model for this purpose. Key ingredients include the determination of the thermal conductivity and pyrolyis law of the matrix, and an accounting of the radiation field generated by the fine aluminum in the gas phase. Experimental results of Dokhan et al. ("The Ignition of Ultra-Fine Aluminum in Ammonium Perchlorate Solid Propellant Flames," AIAA Paper 2003-4810, July 2003) are used for calibration and in comparisons.

I. Introduction

In recent years we have constructed and tested numerical models of heterogeneous propellant combustion, with a specific focus on HTPB/AP propellants [1–3]. One of the characteristics of these models is the specification of the propellant surface location by the formula

$$y = f(x, z, t) \tag{1}$$

where f is single-valued. Because the surface regresses in the normal direction at a speed r_b, where r_b is the burning rate, f satisfies the kinematic equation

$$f_t + r_b\sqrt{1 + (f_x)^2 + (f_z)^2} = 0 \tag{2}$$

No special strategies are needed to couple this equation with the description of the heat conduction in the solid ($y < f$), and the description of the combustion field in the region $y > f$.

However, there are circumstances for which the single-valued specification (1) is not correct, the most important of which arise when the propellant contains aluminum, the particles of which create a complex topography as they pass through the surface. The value of aluminized propellants is well established and one of our goals is to extend the work of [2,3] to such propellants. To do this requires a level-set strategy in place of Eqs. (1) and (2), a strategy of the kind discussed in [4,5]. This has successfully been implemented for the two-dimensional (planar) problem [6,7], and we expect to report soon on the three-dimensional problem.

The aluminum particles added to the propellants can vary widely in size, and recently there has been a significant interest in ultrafine aluminum (Alex) with particles of order 10^{-1} μm in diameter. We are interested in propellants that contain Alex and conventionally sized aluminum ($\sim$20 μm diameter), and the computational domains of interest are typically 200 μm in size. Then the conventional particles can be numerically resolved, but the small ones cannot. Thus, to account for the small particles, it is necessary to homogenize them into the binder, to assume that the binder and the small particles are constituents of a homogeneous blend. In earlier work we examined the homogenization of small AP particles with the binder [8]. Here we consider the homogenization of both AP and aluminum with the binder, and examine how the blend burns. The experimental results reported by Dokhan et al. [9] are used for calibration and comparison.

In due course, with the one-dimensional burning of blends successfully calibrated, we shall add numerically resolvable AP particles and aluminum particles to the blend and carry out three-dimensional calculations of the burning of realistic aluminized heterogeneous propellants. We expect to report on such calculations in a future publication.

II. Experiments of Dokhan et al.

In [9], Dokhan et al. examine the combustion of propellants comprising coarse AP and aluminum embedded in a matrix of binder (PBAN), fine AP, and ultrafine aluminum. The total mass loading of AP is 71% and that of aluminum 18%, so that 11% is binder. 3.6% of the total propellant mass is ultrafine aluminum (diameter $\sim$0.1 μm), and the remaining 14.4% is coarse. Various choices are made for the fraction of fine AP, and Table 1 defines three matrix compositions labeled M27R, M28, and M29. We are concerned with how these burn, and experimental data are reported in [9]. We shall model the combustion within a one-dimensional (homogenized) framework.

Images of the combustion field for each matrix burning at a pressure of 69 atm are shown in [9], and we reproduce those in Fig. 1 (with permission). Each frame is approximately 3 mm high. M27R burns in a highly irregular fashion, with pieces of the propellant breaking off from the surface; there is no bright region and the image can be divided into two domains, one of propellant (blue) and the remainder a red combustion field. On the other hand, for M28 and M29 there are three domains: the propellant (simply connected, unlike that of M27R), a red field starting some 2–3 mm above the propellant surface, and a bright region of intense radiation between the surface and the red region. The intense radiation is generated by the ultrafine aluminum. Reported flame temperatures are 2340 K (M28) and 2625 K (M29).

III. Properties of the Blend

We have earlier discussed homogenization strategies for nonaluminized propellants [8]. These are needed when there is a significant fraction of fine AP, the particles of which cannot be numerically resolved. Within the framework that we have adopted to model heterogeneous propellant combustion, two properties of the blend are required: the effective thermal conductivity and the effective pyrolysis law relating the regression rate to the surface temperature. Here we consider how the earlier results should be modified when aluminum is included in the mix. We start with the pyrolysis law.

Consider pyrolysis laws for pure AP and for pure binder in the form

$$r_{b,\mathrm{AP}} = A_{\mathrm{AP}}e^{-E_{\mathrm{AP}}/R_uT_s}, \qquad r_{b,B} = A_be^{-E_B/R_uT_s} \tag{3}$$

Received 26 August 2005; revision received 14 March 2006; accepted for publication 20 March 2006.

*E-mail: limey@uiuc.edu

Table 1 Mass and volume percentages for the matrix of fine AP and ultrafine aluminum embedded in fuel binder

Matrix	Binder %		AP %		Al %	
	Mass	Volume	Mass	Volume	Mass	Volume
M27R	38.19	58.12	49.31	35.40	12.50	6.48
M28	25.58	42.92	66.05	52.29	8.37	4.79
M29	21.96	37.97	70.86	57.80	7.18	4.23

where R_u is the universal gas constant and T_s is the surface temperature. It was shown in [8] that an effective law for a binder/AP blend is

$$r_{b,\text{blend}} = A_{\text{blend}} e^{-E_{\text{blend}}/R_u T_s} \tag{4}$$

where

$$A_{\text{blend}} = (A_{\text{AP}})^{t_{\text{AP}}} (A_B)^{t_B}, \qquad E_{\text{blend}} = t_{\text{AP}} E_{\text{AP}} + t_B E_B \tag{5}$$

Here, t_{AP} is the volume fraction of AP and $t_B = 1 - t_{\text{AP}}$ is the volume fraction of binder.

Clearly the aluminum, by itself, does not have a meaningful pyrolysis law, and so the extrapolation of these results to aluminized propellants is not straightforward. And so, because the volume of aluminum that we need to consider is small (Table 1) we do not modify these results, merely noting that $t_{\text{AP}} + t_B$ now equals $1 - t_{\text{alum}}$.

A strategy of neglect is appropriate for the pyrolysis law, but not for the conductivity because aluminum conducts so very well. The formulas derived in [8] for a two-material blend are

$$\begin{aligned} 1 &= (1-t)^2 \left(\frac{1-x}{f-x}\right)^2 f \quad \text{in 2D} \\ 1 &= (1-t)^3 \left(\frac{1-x}{f-x}\right)^3 f \quad \text{in 3D} \end{aligned} \tag{6}$$

Here f is the ratio of the thermal conductivity of the blend to the binder, x is the ratio of the thermal conductivity of the AP to the binder, and t is the volume fraction of AP. Thus, when $t = 0$ (no AP) we have $f = 1$ (the conductivity is that of the binder), and when $t = 1$ (no binder) we have $f = x$ (the conductivity is that of the AP).

These results are valid for a distribution of particle sizes, and underlying them is the assumption that

$$\frac{\lambda_{\text{blend}}}{\lambda_B} = f\left(t, \frac{\lambda_{\text{AP}}}{\lambda_B}\right) \tag{7}$$

where $\lambda_{(\cdot)}$ is a conductivity. If we now add aluminum particles to the propellant and assume that Eq. (7) can be extended to

$$\frac{\lambda_{\text{blend}}}{\lambda_B} = f\left(t_{\text{AP}}, t_{\text{alum}}, \frac{\lambda_{\text{AP}}}{\lambda_B}, \frac{\lambda_{\text{alum}}}{\lambda_B}\right) \tag{8}$$

then Eqs. (6) can be applied recursively. By that we mean that we first calculate the conductivity of the two-component system AP in binder (an intermediate value λ_{inter}), and then calculate the conductivity of the two-component system of aluminum embedded in blend. It is not at all clear within the mathematical framework that inverting this process (blending the aluminum and binder first) would generate identical results, but a number of spot checks within the parameter ranges of interest show that the differences are negligible.

Fig. 1 Combustion field images. Left: M27R, middle: M28, right: M29.

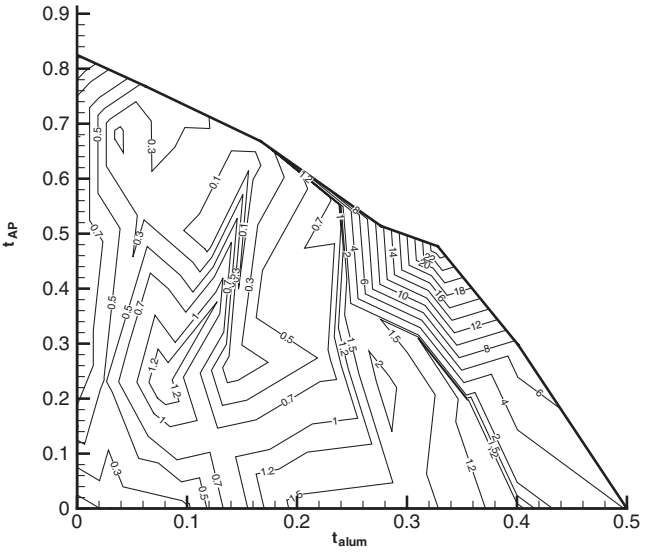

Fig. 2 Percent error contours $|(\lambda_{\text{analytical}} - \lambda_{\text{numerical}})/\lambda_{\text{numerical}}| \times 100$, two dimensions.

As in [8] the predictions can be tested numerically. It is only necessary to take a square or cube of propellant, apply a temperature difference across two opposite faces (the other faces are insulated) and determine the heat flux between the two faces via integration of the equation

$$\nabla \cdot (\lambda \nabla T) = 0 \tag{9}$$

Figure 2 is a contour plot in the $t_{\text{alum}} - t_{\text{AP}}$ plane of the errors for the two-dimensional case, and Fig. 3 shows the three-dimensional results. An absolute upper boundary for these plots is the straight line

$$t_{\text{AP}} = t_{\max} - t_{\text{alum}}$$

where $t_{\max}$ is the maximum volume fraction that can be packed by spheres (approximately 0.82), but we show smaller domains (bounded by the upper thick lines) for computational reasons (the calculations are time-consuming) and because the range of values of

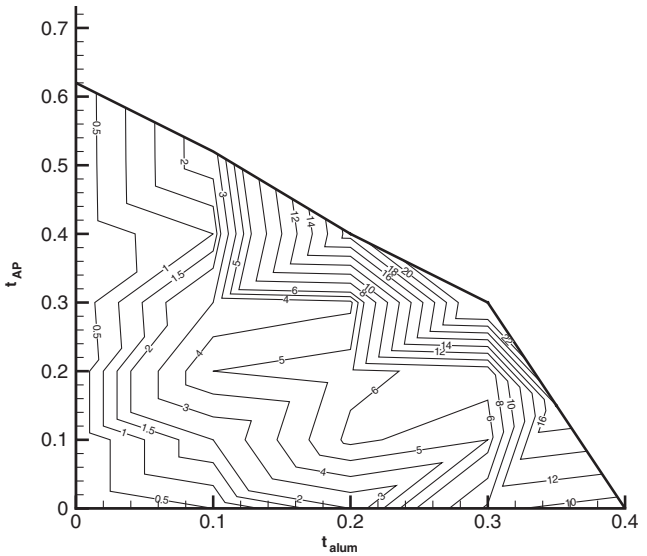

Fig. 3 Percent error contours $|(\lambda_{\text{analytical}} - \lambda_{\text{numerical}})/\lambda_{\text{numerical}}| \times 100$, three dimensions.

Table 2 Ratio of λ_{blend} to λ_{inter} for $t_{\text{AP}} = 0.6$

t_{alum}	0	0.05	0.1	0.15	0.2
2-D	1	1.108	1.234	1.382	1.560
3-D	1	1.165	1.369	1.623	1.943

t_{alum} that are of interest is quite limited. For example, a matrix that contains more than about 12% of Alex does not have enough mechanical integrity for use as a rocket propellant.[†]

These results show that the strategy is highly accurate when only AP is present, and acceptably accurate when only aluminum is present. The largest errors when both are present occur in the neighborhood of $t_{\text{alum}} = 0.3$, $t_{\text{AP}} = 0.4$ (two-dimensional), $t_{\text{AP}} = 0.3$ (three-dimensional). The errors are small for the compositions listed in Table 1, and for the compositions that we shall use in our subsequent three-dimensional calculations.

That the aluminum plays a significant role in defining the conductivity of the matrix is clear from Table 2, which lists the ratio of λ_{blend} to λ_{inter} for $t_{\text{AP}} = 0.6$, where λ_{blend} is the conductivity of the matrix of all three components, and λ_{inter} is the intermediate value in the recursive application of Eqs. (6), the conductivity of the combined AP and binder.

One of the reviewers of this paper noted that aluminum is coated with oxide, and so raised the interesting question of whether this is of consequence to the conductivity when the aluminum particles are extremely small. We believe that this is not the case, given the fact that the conductivities of aluminum (204.1 $\text{W/m} \cdot \text{K}$) and aluminum oxide (50 $\text{W/m} \cdot \text{K}$) are so much larger than that of both the AP (0.405 $\text{W/m} \cdot \text{K}$) and the binder (0.276 $\text{W/m} \cdot \text{K}$). Thus, both the conductivity of the aluminum and the oxide can be assigned the value of infinity without significantly affecting the effective conductivity of the propellant. This can be explicitly seen by examining the one-dimensional problem of conduction through layers of AP, aluminum, and oxide. Suppose, for example, that the AP layer has thickness 100, the aluminum layer has thickness 20, and the oxide layer has thickness 4. Then the effective conductivity of the three layers combined is

$$\frac{100 + 20 + 4}{100/0.405 + 20/204.1 + 4/50}$$

with a value of 0.502, some 24% larger than that of pure AP. But if the conductivities 204.1 and 50 in this formula are replaced by infinity, then again the value, to within three significant figures, is 0.502.

It should be noted that the pyrolysis law (4) and (5) modified with

$$t_B = 1 - t_{\text{AP}} - t_{\text{alum}} \tag{10}$$

has not been tested numerically because, at the present time, we do not have a three-dimensional code that can handle the emergence of aluminum particles at the surface. Thus the validation strategy of [8] is not yet possible.

Before leaving this section it may be noted that there are, in the literature, a large number of homogenization formulas for properties such as thermal conductivity, and some may be superior to the one we have used here. But that is not easy to determine. Many of the formulas are not validated or are validated against a limited set of experimental data. For some purposes an experimental comparison is the one to make, but when, as here, the formulas are a substitute for computation, appropriate validation comes from comparison with computational data. And so, because the present study does not have as its subject the thermal conductivity of heterogeneous materials, and we merely need a formula sufficiently accurate for our purposes, we shall be content with the present strategy.

[†]Blomshield, F., China Lake, personal communication, June 2004.

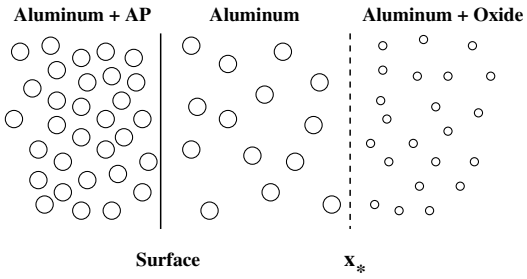

Fig. 4 The model.

IV. Simulation of One-Dimensional Burning of the Blend

In this section we formulate a one-dimensional model to describe the combustion of the binder/AP/aluminum blend or matrix. In the solid phase there is heat conduction with an effective conductivity, surface regression is governed by an effective pyrolysis law, and the gas-phase is characterized by a three-step kinetic scheme corresponding to the well-known Beckstead–Derr–Price (BDP) [10] model for heterogeneous propellant combustion. In addition, radiation is accounted for, originating in the aluminum (cf. Fig. 1).

Some elementary characteristics of the model are indicated in Fig. 4. Within the solid there are AP and aluminum particles, in a gas-layer contiguous with the surface there are only aluminum particles, and beyond this layer there are aluminum and aluminum oxide particles. The layer lies in the interval $[0, x_*]$, and x_* is an assigned parameter. The manner in which it is chosen is discussed later.

An important characteristic of our model is that certain phenomena that occur in a thin surface layer (heterogeneous reaction and in-depth radiation absorption) are modeled by pure surface physics: a pyrolysis law and surface absorption. The processes that occur in the surface layer are not well understood qualitatively or quantitatively and, indeed, provide one of the major challenges of "exact" modeling of propellant burning, and, until better understood, one best bypassed.

A. The Gas-Phase Equations

The three-step kinetics model is one that we have used in our multidimensional simulations [3], and an accounting of the manner in which the parameters are chosen may be found there. We have

$$\begin{aligned} &\text{AP}\,(X) \xrightarrow{R_1} \text{decomposition products}(Z) \\ &\beta X + \text{binder}(Y) \xrightarrow{R_2} \text{final products} \\ &\beta Z + \text{binder}(Y) \xrightarrow{R_3} \text{final products} \end{aligned} \tag{11}$$

where

$$\begin{aligned} R_1 &= D_1 P_o^{n_1} X \exp\{-E_1/R_u T\} \\ R_2 &= D_2 P_o^{n_2} X^{3.3} Y^{0.4} \exp\{-E_2/R_u T\} \\ R_3 &= D_3 P_o^{n_3} YZ \exp\{-E_3/R_u T\} \end{aligned} \tag{12}$$

R_2 corresponds to the primary diffusion flame of the BDP model, and R_3 corresponds to the secondary diffusion flame, although in the homogenized treatment here there are no diffusion flames of course.

The corresponding quasi-steady equations for the species X, Y, Z and the temperature T are

$$\mathcal{L}(X, Y, Z) = (-R_1 - \beta R_2, -R_2 - R_3, R_1 - \beta R_3) \tag{13}$$

$$\mathcal{L}(T) = -\frac{1}{c_p}\frac{\mathrm{d}q_r}{\mathrm{d}x} + (Q_{g1}R_1 + Q_{g2}R_2 + Q_{g3}R_3)/c_p \tag{14}$$

where

$$\mathcal{L} \equiv M\frac{\mathrm{d}}{\mathrm{d}x} - \frac{\mathrm{d}}{\mathrm{d}x}\left(\frac{\lambda_g}{c_p}\frac{\mathrm{d}T}{\mathrm{d}x}\right) \tag{15}$$

Here, q_r is the gas-phase radiative heat flux, to be discussed later, and $M = \rho_s r_b$ is the mass flux, with r_b the burning rate and ρ_s the solid phase density, the latter given by

$$\rho_s = \rho_{\mathrm{AP}} t_{\mathrm{AP}} + \rho_{\mathrm{alum}} t_{\mathrm{alum}} + \rho_B t_B \tag{16}$$

All Lewis numbers are assumed to be unity, but temperature dependent transport is accounted for, viz. [11]

$$\lambda_g = 1.08 \times 10^{-4} T + 0.0133 \ \mathrm{W/m \cdot K} \tag{17}$$

when T is assigned in degrees Kelvin. The specific heat c_p is assumed to be constant. And the parameter β in Eq. (13) is the overall mass-based AP/binder stoichiometric ratio: β kilograms of AP(X) are required for the stoichiometric consumption of 1 kg of binder (Y). We do not account for the contribution that the aluminum makes to the conductivity within the gas phase, simply because we do not know how to do this correctly. The aluminum particles are not simply passive ingredients, but burn and radiate, and it seems unlikely that a simple volume averaging, as adopted in [12], for example, can be justified. Fortunately, our model includes some parameters that must be calibrated, and errors in λ_g will be absorbed in this way.

Boundary conditions for X, Y, Z, T are

$$\begin{aligned} &\text{at } x = 0\text{: } M(X_i - X_{i,s}) - \frac{\lambda_g}{c_p}\frac{\mathrm{d}X_i}{\mathrm{d}x} = 0, \qquad X_i = (X, Y, Z) \\ &\lambda_g \frac{\mathrm{d}T}{\mathrm{d}x} - c_p M(T - T_0) + Q_s M - q_r = 0 \end{aligned} \tag{18}$$

where T_o is the supply temperature in the solid at $x \to -\infty$, and the $\{X_{i,s}\}$ are mass fractions in the solid defined by the solid composition. Also

$$\text{as } x \to \infty\text{: } \frac{\mathrm{d}X_i}{\mathrm{d}x} \to 0, \qquad \frac{\mathrm{d}T}{\mathrm{d}x} \to 0 \tag{19}$$

Table 3 lists the parameters used in the study.

Table 3 Parameter values

Parameter	Value	Unit
A_{AP}	1.45×10^5	cm/s
A_B	1.036×10^3	cm/s
c_p	0.3	kcal/kg · K
D_1	4.11×10^1	$\mathrm{gm \cdot cm^{-3} \cdot s^{-1} \cdot bar^{-n_1}}$
D_2	2.35×10^4	$\mathrm{gm \cdot cm^{-3} \cdot s^{-1} \cdot bar^{-n_2}}$
D_3	9.50×10^1	$\mathrm{gm \cdot cm^{-3} \cdot s^{-1} \cdot bar^{-n_2}}$
E_{AP}/R_u	11,000	K
E_B/R_u	7,500	K
E_1/R_u	3,000	K
E_2/R_u	8,500	K
E_3/R_u	8,500	K
n_1	2.06	——
n_2	2.06	——
n_3	1.60	——
$Q_{s,\mathrm{AP}}$	−80	kcal/kg
$Q_{s,B}$	−66	kcal/kg
Q_{g1}	410	kcal/kg
Q_{g2}	7,403	kcal/kg
Q_{g3}	4,396	kcal/kg
T_o	300	K
λ_{AP}	0.405	W/m · K
λ_{Al}	204.1	W/m · K
λ_B	0.276	W/m · K
ρ_{AP}	1,950	$\mathrm{kg/m^3}$
ρ_{Al}	2,700	$\mathrm{kg/m^3}$
ρ_B	920	$\mathrm{kg/m^3}$
β	7.33	——

B. Equations for the Radiative Flux

We assume that the gas phase can be approximated by a gray medium, and use the two-stream or two-flux model so that the radiative heat flux is given by

$$q_r = \pi(I^+ - I^-) \tag{20}$$

where πI^+ is the flux moving away from the surface and πI^- is the flux moving towards the surface. The equations governing I^+ and I^- are

$$\begin{aligned} \frac{\mathrm{d}I^+}{\mathrm{d}x} + (s + a)I^+ &= eI_b + sI^- \\ -\frac{\mathrm{d}I^-}{\mathrm{d}x} + (s + a)I^- &= eI_b + sI^+ \end{aligned} \tag{21}$$

where s is the scattering coefficient, a the absorption coefficient, and e the emission coefficient. I_b is the blackbody intensity, given by

$$I_b = \sigma T^4/\pi \tag{22}$$

with $\sigma = 5.67 \times 10^{-12}$ $\mathrm{W/cm^2 \cdot K^4}$, the Stefan-Boltzmann constant.

When I^- is eliminated between Eqs. (21) we have

$$\frac{\mathrm{d}^2 I^+}{\mathrm{d}x^2} = [(s + a)^2 - s^2]I^+ + e\frac{\mathrm{d}I_b}{\mathrm{d}x} - (a + 2s)eI_b \tag{23}$$

and once this is solved, I^- can be found from the first Eq. (21). It is also possible, as is well known, to derive an equation for q_r from (20) and (21), viz.

$$\frac{\mathrm{d}^2 q_r}{\mathrm{d}x^2} = 2\pi e\frac{\mathrm{d}I_b}{\mathrm{d}x} + a(a + 2s)q_r \tag{24}$$

the well-known Eddington approximation, e.g., [13]. If we set $a = s = 1$, $e = 2L$, where L is a length, and consider the limit $L \to 0$, we get

$$q_r = -\frac{2\pi e}{a(a + 2s)}\frac{\mathrm{d}I_b}{\mathrm{d}x} \equiv -\frac{4}{3}L\sigma\frac{\mathrm{d}T^4}{\mathrm{d}x} \tag{25}$$

corresponding to the optically thick limit. And in the limit $L \to \infty$,

$$\frac{\mathrm{d}q_r}{\mathrm{d}x} = 2\pi e(I_b + \mathrm{const}) \equiv 4L\sigma\left(T^4 - T_\infty^4\right) \tag{26}$$

corresponding to the optically thin limit.

Insofar as Eq. (24) is concerned, the boundary conditions are

$$q_r(0) = q_o, \qquad \frac{\mathrm{d}q_r}{\mathrm{d}x}(\infty) = 0 \tag{27}$$

where q_o is chosen so that equilibrium prevails far from the surface and $q_r(\infty) = 0$. And insofar as I^+ is concerned we have

$$\text{at } x = 0\text{: } I^+ = 0, \qquad \text{as } x \to \infty\text{: } \frac{\mathrm{d}I^+}{\mathrm{d}x} \to 0 \tag{28}$$

We assume that the propellant surface is nonreflecting and nonemitting.

C. Radiation Parameters

The parameters of the radiation model are adapted from the discussion of Brewster and Parry [14] for aluminum of conventional size. Thus

$$\begin{aligned} a &= \frac{3t_{\mathrm{oxide}}\alpha_{\mathrm{oxide}}}{D_{\mathrm{oxide}}} + k_1\frac{3t_{\mathrm{alum}}\alpha_{\mathrm{alum}}}{D_{\mathrm{alum}}} \\ s &= \frac{3t_{\mathrm{oxide}}\hat{\rho}_{\mathrm{oxide}}B_{\mathrm{oxide}}}{D_{\mathrm{oxide}}} + k_1\frac{3t_{\mathrm{alum}}\hat{\rho}_{\mathrm{alum}}B_{\mathrm{alum}}}{D_{\mathrm{alum}}} \\ e &= \frac{3t_{\mathrm{oxide}}\epsilon_{\mathrm{oxide}}}{D_{\mathrm{oxide}}} + k_1\frac{3t_{\mathrm{alum}}\epsilon_{\mathrm{alum}}}{D_{\mathrm{alum}}} \end{aligned} \tag{29}$$

Table 4 Radiation parameter values from [14]

	α	$\hat{\rho}$	ϵ	B	D, μm
Al	0.10	0.90	1.00	0.5	1.0
Al_2O_3	0.45	0.55	0.45	0.3	0.3

where t_{alum} and t_{oxide} are the volume fractions of aluminum and aluminum oxide (Al_2O_3); α, $\hat{\rho}$, ϵ, and B are the two-flux absorption, reflection, emission, and back-scatter-fraction coefficients; and k_1 is an empirical constant that is introduced because of uncertainties in the values of α_{alum}, $\hat{\rho}_{\text{alum}}$, B_{alum}, ϵ_{alum}, and the diameter D_{alum}. The values we have chosen are listed in Table 4 [14].

The volume fractions that appear in Eqs. (29) are defined by the formulas

$$t_{\text{alum}} = \begin{cases} ts_{\text{alum}} & 0 < x < x_* \\ ts_{\text{alum}} e^{-(x-x_*)\Gamma} & x_* < x < \infty \end{cases}$$
$$t_{\text{oxide}} = \begin{cases} 0 & 0 < x < x_* \\ k_2 ts_{\text{alum}} (1 - e^{-(x-x_*)\Gamma}) & x_* < x < \infty \end{cases} \tag{30}$$

where ts_{alum} is the volume fraction of the aluminum in the solid, k_2 is an empirical constant that reflects the uncertainty in the amount of oxide produced from the combustion of Alex, and Γ is a decay constant.

V. Calculations

A. Benchmark Calculations

The five second-order differential Eqs. (13–15) and (23) are solved for the five unknowns (X, Y, Z, T, I^+), subject to the boundary conditions (18), (19), and (28), using the two-point boundary value solver COLSYS. The grid is nonuniform where x is positive, and the first grid point off the surface is at $x = 0.5$ μm or less. Grid resolution checks have been carried out to ensure grid independence of the solutions.

The parameters so far unspecified that must be chosen are k_1, k_2, Γ, and x_*. We start with: $k_1 = 0.2, k_2 = 0.015 \times (P/13)$ where P is the pressure in atmospheres, $\Gamma = 10$, and x_* is taken to be the point where the reaction rate R_2 is equal to 0.001. These choices are partly motivated by the following: k_1 is chosen to roughly match the M29 data point at low pressure, the pressure dependence of k_2 arises because of evidence that the volume fraction of oxide doubles if the pressure is doubled [14], and the near vanishing of R_2 is a measure of the distance over which the temperature rises in the combustion field, leading to the combustion of the aluminum. These choices are plausible but in some sense arbitrary, and what matters primarily is whether they yield sensible results. Later we will show the results of sensitivity tests in which the parameters are altered from these benchmark values.

Figures 5–10 show the results for the benchmark case. Figure 5 compares the burn rates predicted by the model to those of Dokhan

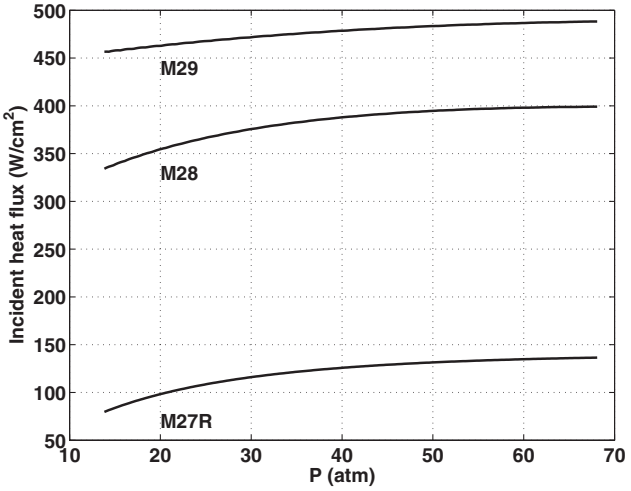

Fig. 6 Incident radiant heat flux at the surface. Benchmark case.

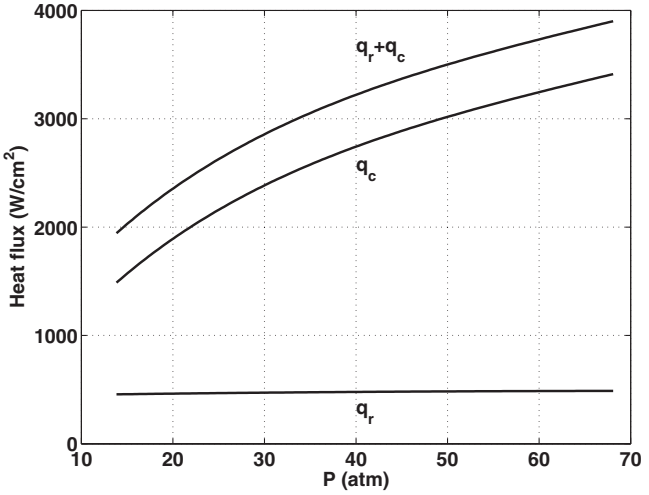

Fig. 7 Radiative and conductive heat fluxes to the surface for the matrix M29.

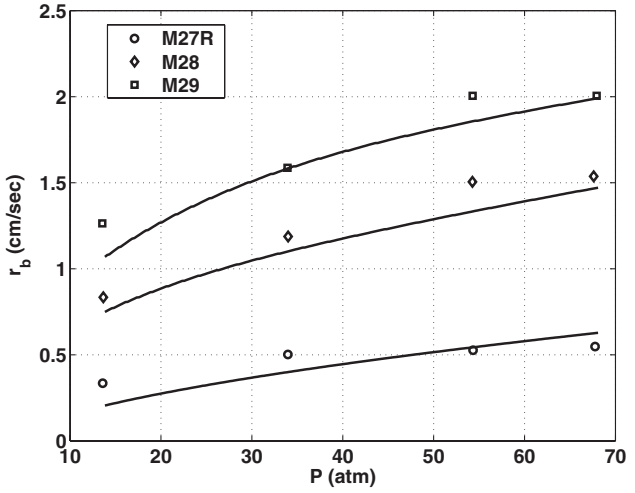

Fig. 5 Burn rate vs pressure. Symbols: data of Dokhan et al. [9]; curves: numerical simulations. Benchmark case.

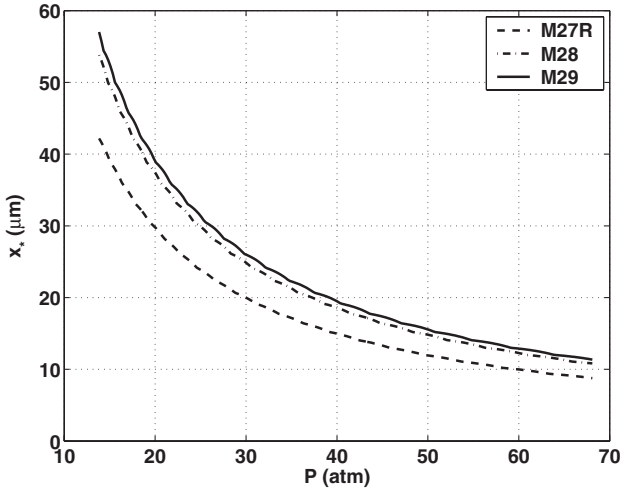

Fig. 8 x_* in microns vs pressure, benchmark case. x_* is the point where R_2 has fallen to 0.001.

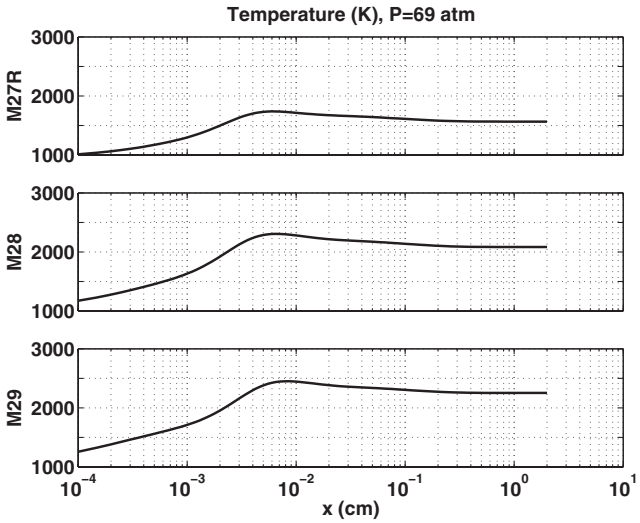

Fig. 9 Temperature vs distance, benchmark case.

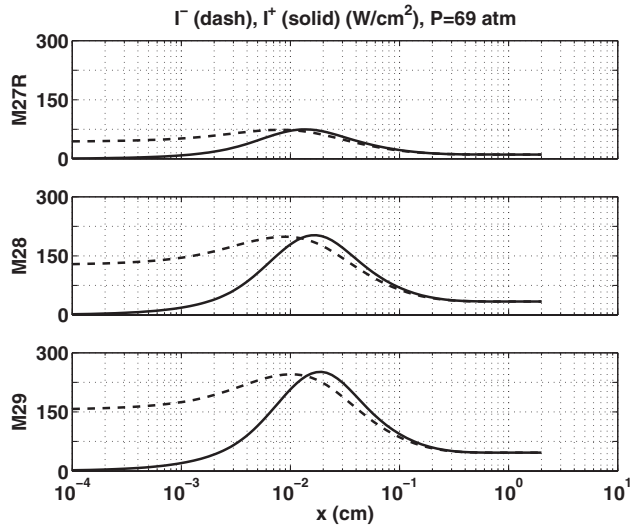

Fig. 10 I^- and I^+ as vs distance, benchmark case.

et al. [9], and satisfactory agreement is achieved, despite the significant variations in the makeup of each matrix. This agreement means that we can use the model as an ingredient of three-dimensional calculations for propellants that contain coarse AP and aluminum in addition to the fine material.

The incident radiant heat flux at the surface, $\pi I^-(0)$, is plotted as a function of pressure in Fig. 6. Note that the weak radiative flux for the matrix M27R is consistent with the first panel of Fig. 1. The range of values shown in Fig. 6 are consistent with the range of values reported in [12] in a study of bimodal AP with fine aluminum particles.

The contribution that radiation makes to the total heat flux (radiative and conductive) for M29 is apparent from Fig. 7. The conductive flux is much larger than the radiative flux, but the latter is not negligible, particularly at the lower pressures.

Values of x_* are plotted as a function of pressure in Fig. 8. Recall that x_* is defined by the decay of R_2, and so the decay with pressure is easily understood.

The temperature distribution at a pressure of 69 atm is shown in Fig. 9. For each matrix the maximum occurs at a distance of approximately 60 μm from the surface; the final (equilibrium) values differ from the experimental values reported in [9] by about 12%.

And the radiation intensities are shown in Fig. 10, from which we can see that radiative equilibrium is achieved at roughly a millimeter or so from the surface.

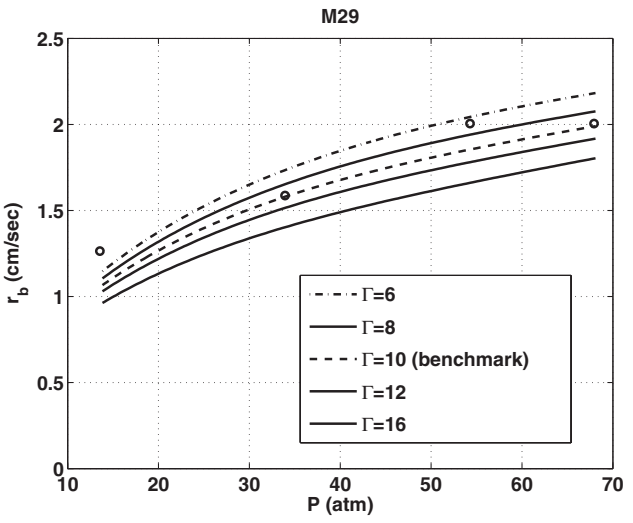

Fig. 11 r_b vs pressure for M29, several values of Γ.

B. Sensitivity Studies

Modeling of the kind carried out here requires us to choose a number of parameters whose values are not well known. This can introduce serious difficulties if the solutions are unduly sensitive to the parameter values, and so it is always wise to carry out sensitivity studies of some kind. Here we shall examine, by direct calculation, variations in the burning rate of M29 (the matrix that burns most vigorously) to changes in the four parameters k_1, k_2, Γ, and x_*. k_1 is an empirical constant used in the radiation ingredients defined by Eq. (29); k_2 is an empirical constant introduced in Eq. (30) because of uncertainties in the aluminum oxidation; Γ is a decay constant, also introduced in Eq. (30), which characterizes the length scale on which the aluminum is converted to oxide; and x_* is defined by Fig. 4, and is controlled by the reaction rate R_2.

The sensitivity calculations are of little intrinsic interest except insofar as they reveal sensitivity or insensitivity, and so our discussion is brief.

Figure 11 shows the effect of varying the decay parameter Γ on the burn rate. The dash line corresponds to the benchmark value $\Gamma = 10$. Burning rates decrease monotonically with increases in Γ with significant sensitivity at the higher pressures, so that a completely predictive tool can only be developed with an accurate description of the combustion of fine aluminum.

Figure 12 shows the effect of varying x_* on the burn rate. These variations are calculated by taking the benchmark value, defined by $R_2 = 0.001$, and multiplying it by 3, 2, or 0.5. There is a

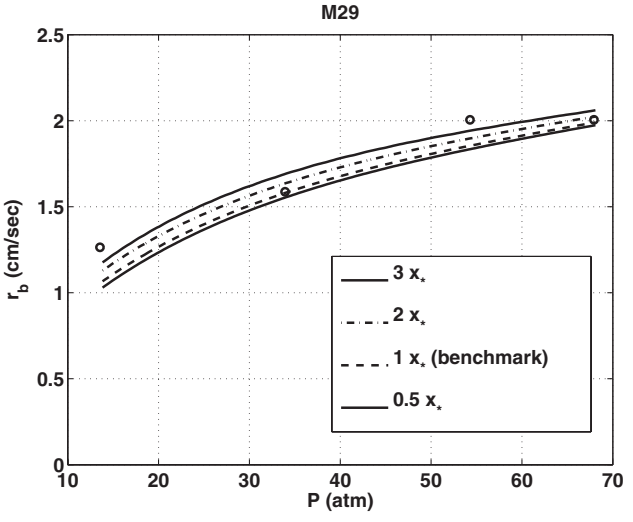

Fig. 12 r_b vs pressure for M29, several values of x_*.

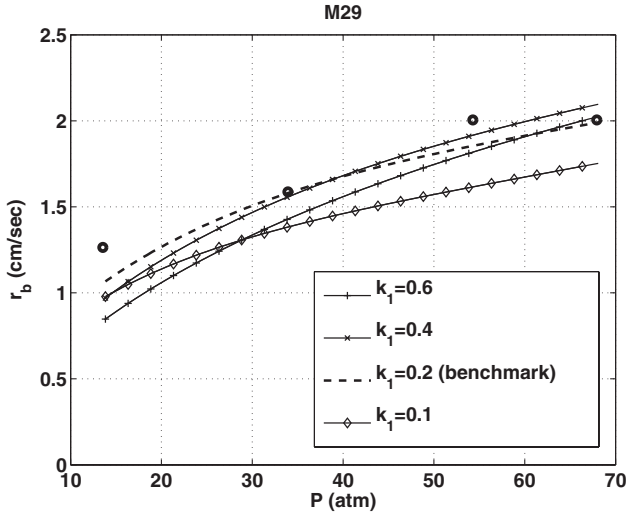

Fig. 13 r_b vs pressure for M29, several values of k_1.

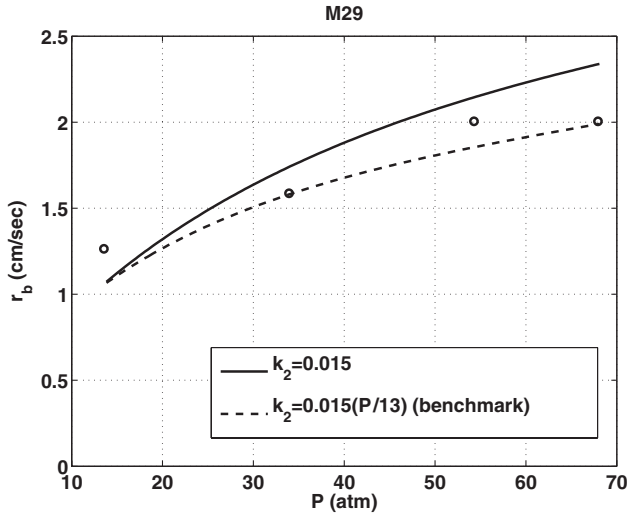

Fig. 14 r_b vs pressure for M29 with and without a k_2 pressure dependence.

lack of sensitivity over this range, a good thing, but the choice of R_2 to define the benchmark case is arbitrary (why not 0.01 or 0.0001?) and over this larger range the effects would be significant. And so, again, it would be of value to have a more detailed and more precisely defined model of the aluminum history after it leaves the surface.

Figure 13 shows the effect of varying k_1, a response that is not monotonic. Doubling it has little effect, but halving it has a significant effect at the higher pressures.

Figure 14 shows what happens when the pressure dependence of k_2 is turned off, and makes clear the necessity of retaining a dependence. And Fig. 15 shows the effect of varying k_2 with the pressure dependence retained.

VI. Conclusions

The work we have described here is part 1 of a study of aluminized propellant combustion, in which we examine to what extent we can model the one-dimensional burning of a matrix of fuel binder, fine aluminum, and fine ammonium perchlorate. It is essential that we be able to do this, as it is an essential component of three-dimensional calculations in which particles that must be resolved numerically are added to the matrix.

The model includes a determination of the thermal conductivity of the matrix from the individual conductivities of its constituents; an accounting of the radiation field, both outgoing and ingoing,

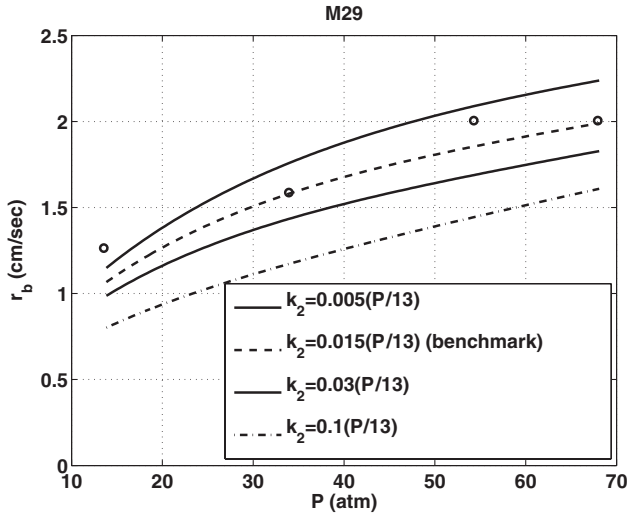

Fig. 15 r_b vs pressure for M29, several values of k_2.

generated by the aluminum particles in the gas phase; and a three-step model for the gas-phase kinetics corresponding to the well-known BDP model [10]. The kinetics parameters were defined and validated in an earlier paper [3].

Dokhan et al. [9] report an experimental study for a number of matrix formulations, and we have used these results to help us assign parameter values, and for comparisons between measured and predicted burning rates. These comparisons are satisfactory. However, it would clearly be of value to formulate a more precise model of the aluminum history and the radiative properties of the aluminum.

Acknowledgment

This work was supported by the U.S. Department of Energy through the University of California under subcontract B341494. In addition, T. L. Jackson and J. Buckmaster are supported by the Air Force Office of Scientific Research.

References

[1] Jackson, T. L., and Buckmaster, J., "Heterogeneous Propellant Combustion," *AIAA Journal*, Vol. 40, No. 6, 2002, pp. 1122–1130.

[2] Massa, L., Jackson, T. L., Buckmaster, J., and Campbell, M., "Three-Dimensional Heterogeneous Propellant Combustion," *Proceedings of the Combustion Institute*, Vol. 29, No. 2, 2002, pp. 2975–2983.

[3] Massa, L., Jackson, T. L., and Buckmaster, J., "New Kinetics for a Model of Heterogeneous Propellant Combustion," *Journal of Propulsion and Power*, Vol. 21, No. 5, 2005, pp. 914–924.

[4] Sethian, J. A., *Level Set Methods and Fast Marching Methods*, Cambridge Monograph on Applied and Computational Mathematics, Cambridge Univ. Press, Cambridge, England, U.K., 1999.

[5] Osher, S., and Fedkiw, R., *Level Set Methods and Dynamic Implicit Surfaces*, Vol. 153, Applied Mathematical Sciences, Springer, New York, 2003.

[6] Wang, X., Jackson, T. L., and Massa, L., "Numerical Simulation of Heterogeneous Propellant Combustion by a Level Set Method," *Combustion Theory and Modeling*, Vol. 8, No. 2, 2004, pp. 227–254.

[7] Wang, X., and Jackson, T. L., "The Numerical Simulation of Two-Dimensional Aluminized Composite Solid Propellant Combustion," *Combustion Theory and Modeling*, Vol. 9, No. 1, 2005, pp. 171–197.

[8] Chen, M., Buckmaster, J., Jackson, T. L., and Massa, L., "Homogenization Issues and the Combustion of Heterogeneous Solid Propellants," *Proceedings of the Combustion Institute*, Vol. 29, No. 22002, pp. 2923–2929.

[9] Dokhan, A., Price, E. W., Seitzman, J. M., and Sigman, R. K., "The Ignition of Ultra-Fine Aluminum in Ammonium Perchlorate Solid Propellant Flames," AIAA Paper 2003-4810, July 2003.

[10] Beckstead, M. W., Derr, R. L., and Price, C. F., "Model of Composite

Solid-Propellant Combustion Based on Multiple Flames," *AIAA Journal*, Vol. 8, No. 12, 1970, pp. 2200–2207.

[11] Rasmussen, B., and Frederick, R. A., Jr., "A Nonlinear Heterogeneous Model of Composite Solid Propellant Combustion," *Journal of Propulsion and Power*, Vol. 18, No. 5, 2002, pp. 1086–1092.

[12] Ishihara, A., Brewster, M. Q., Sheridan, T. A., and Krier, H., "The Influence of Radiative Heat Feedback on Burning Rates in Aluminized Propellants," *Combustion and Flame*, Vol. 84, No. 1, 1991, pp. 141–153.

[13] Modest, M. F., *Radiative Heat Transfer*, McGraw–Hill, New York, 1993.

[14] Brewster, M. Q., and Parry, D. L., "Radiative Heat Feedback in Aluminized Solid Propellant Combustion," *Journal of Thermophysics and Heat Transfer*, Vol. 2, No. 2, 1998, pp. 123–130.

J. Powers
Associate Editor